Neutrinoless double-β decay: Combining quantum Monte Carlo and the nuclear shell model with the generalized contact formalism

Ronen Weiss,[1] Pablo Soriano,[2] Alessandro Lovato,[3,4,5] Javier Menendez,[2] and R. B. Wiringa[3]
[1]*Theoretical Division, Los Alamos National Laboratory, Los Alamos, New Mexico 87545, USA*
[2]*Department of Quantum Physics and Astrophysics and Institute of Cosmos Sciences, University of Barcelona, 08028 Barcelona, Spain*
[3]*Physics Division, Argonne National Laboratory, Argonne, Illinois 60439, USA*
[4]*Computational Science Division, Argonne National Laboratory, Argonne, Illinois 60439, USA*
[5]*INFN-TIFPA Trento Institute of Fundamental Physics and Applications, Via Sommarive, 14, 38123 Trento, Italy*

(Received 3 January 2022; revised 20 August 2022; accepted 24 October 2022; published 7 December 2022)

Neutrinoless double beta decay searches can determine the Majorana nature of neutrinos, the absolute neutrino mass, and provide invaluable insights on the matter dominance of the universe. However, the uncertainty in the nuclear matrix elements that govern the decay limits the physics reach of these experiments. We devise a novel framework based on the generalized contact formalism that combines the nuclear shell model and quantum Monte Carlo methods and compute the neutrinoless double-beta decay of nuclei used in the most advanced experiments, including ^{76}Ge, ^{130}Te, and ^{136}Xe. Our results cover all relevant terms, including the leading-order short-range operator recognized recently. We validate our method in light nuclei by comparing against accurate variational Monte Carlo results. On heavy systems we obtain reduced nuclear matrix elements compared with previous calculations due to additional correlations captured by quantum Monte Carlo and introduced within the generalized contact formalism, suggesting longer decay half-lives than previously considered. On the other hand, we find an enhancement of the nuclear matrix elements due to the new short-range operator.

DOI: 10.1103/PhysRevC.106.065501

I. INTRODUCTION

Neutrinoless double-beta decay ($0\nu\beta\beta$) is a hypothetical transition of atomic nuclei forbidden by the standard model of particle physics, in which two neutrons are transmuted into two protons and two electrons are emitted with no accompanying antineutrinos [1]. The measurement of $0\nu\beta\beta$ decay would have profound implications, demonstrating that lepton number is not a symmetry of nature, proving that the neutrino mass has a Majorana component [2]—so that neutrinos and antineutrinos are the same particle—and, since two matter particles are created without the corresponding antimatter ones, illuminating the matter dominance in the universe. In addition, assuming the decay is mediated by the exchange of light neutrinos—the best motivated scenario both experimentally and theoretically—it would provide invaluable insight on the neutrino mass scale and ordering [3,4].

Because $0\nu\beta\beta$ is a second-order decay, in practice it can only be detected in the few nuclei where β decay is either energetically forbidden or strongly suppressed by spin change. Current best limits are given for ^{76}Ge ($T^{0\nu}_{1/2} > 1.8 \times 10^{26}$ yr [5]) and ^{136}Xe ($T^{0\nu}_{1/2} > 1.07 \times 10^{26}$ yr [6]), and in this decade next-generation ton-scale experiments plan to reach $T^{0\nu}_{1/2} \approx 10^{28}$ yr, mainly in ^{76}Ge, ^{100}Mo, ^{130}Te, or ^{136}Xe [7–10]. Since the decay involves physics beyond the standard model, its rate is proportional to a parameter describing the lepton number violation in that beyond standard model mechanism. In addition, the decay rate is also governed by a nuclear matrix element (NME) that encodes the structure of the initial and final nuclei. Thus, extracting specific new physics information from half-life measurements demands reliable NMEs and hence high-quality nuclear structure studies of heavy nuclei, such as ^{76}Ge and ^{136}Xe.

Most NME calculations use the quasiparticle random-phase approximation (QRPA) [11–14], nuclear shell model (SM) [15–18], energy density functional theory [19–22], or the interacting-boson model [23,24]. Among them, the SM describes very well a variety of nuclear structure properties of medium and heavy nuclei including those involved in $0\nu\beta\beta$ decay [25–27]. These properties are mostly dictated by nucleons around the Fermi surface, and therefore dominated by mid- and long-range correlations. However, the SM and the many-body methods listed above show deficiencies related to the inconsistent treatment of the $0\nu\beta\beta$-decay operator—for an extensive review see Ref. [28]. These may appear as missing nuclear correlations or two-nucleon currents in the decay operator.

Ab initio many-body methods, in contrast, treat transition operators consistently, as they describe nuclear properties emerging from the bare interaction between protons and neutrons. This way they reproduce well β-decay rates in light- and medium-mass nuclei [29] without any adjustments (usually known as "quenching"), a feature required by the less sophisticated many-body approaches mentioned above

[23,30–33]. The challenge for *ab initio* approaches is to describe heavy nuclei like those that $\beta\beta$ decay. *Ab initio* methods relying on single-particle basis expansion have calculated reliably the $0\nu\beta\beta$-decay NME for ^{48}Ca [34–36], and have even been extended to the heavier ^{76}Ge and ^{82}Se [37] but with nuclear properties not yet of the same quality as in SM calculations. On the other hand, quantum Monte Carlo (QMC) methods [38] use coordinate-space representation of many-body wave functions and are well-suited for the description of nuclear states with complex intrinsic structures [39]. In particular, they accurately treat short-range nuclear dynamics, a key aspect for $0\nu\beta\beta$ transitions where decaying neutrons are typically a few fm apart. This is even more critical for the contribution to the NME recently recognized in Refs. [40,41], which is of even shorter-range character. QMC calculations describe well β decays [42] but so far have been limited to light nuclei with up to $A \leqslant 12$ nucleons for $0\nu\beta\beta$ NMEs [40,43].

The generalized contact formalism (GCF) is a powerful tool to model the short-range behavior of nuclear distributions, both in coordinate and momentum space [44–47]. Nuclear wave functions show a universal short-range behavior determined by the nuclear interaction; the only dependence on the specific nucleus comes about as an overall normalization factor, proportional to the number of short-range correlated (SRC) pairs. Hence, the GCF is applicable across the nuclear chart, provided that these normalization factors are known. The GCF has been used to describe quantities that are governed by short-range physics, with negligible long-range contribution.

In this work, we develop a framework that combines the GCF with QMC and the SM to capture both short- and long-range nuclear dynamics that is applicable for a wide range of processes, including $0\nu\beta\beta$ decay. This framework is based on the observation that the ratio of the GCF normalization factors for different nuclei is largely independent of the specific nuclear Hamiltonian. Therefore, the short-range behavior of $0\nu\beta\beta$ transition densities of a given heavy nucleus can be completely determined from state-of-the-art variational Monte Carlo (VMC) and SM calculations of light nuclei, supplemented by SM results for the heavy nucleus of interest. To obtain the full transition density, we rescale the SM predictions so that they continuously match the GCF at short distances. Although similar in spirit to correcting SM transition densities with Jastrow correlations [48–51], our approach is more systematic and can exactly reproduce the transition density at short distance.

First we validate our method in light nuclei, where accurate QMC calculations are available. We then make NME predictions for nuclei used in $0\nu\beta\beta$ experiments, including ^{48}Ca, ^{76}Ge, ^{130}Te, and ^{136}Xe. Our results include estimates of the theoretical uncertainty associated with our method, although not all uncertainty sources can be currently accounted for. In addition to the contribution of long-range operators to the NME, calculated in most previous works, we include the contribution of the recently acknowledged short-range operator, for which our approach may be particularly reliable. We follow recent analyses and estimate the hadronic coupling associated with this short-range term by the charge-independence-breaking (CIB) term of the Argonne v_{18} (AV18) potential used in the VMC calculations. While for this work we use the phenomenological AV18 plus the three-nucleon Urbana X (UX) force, our method is general and can readily be applied to interactions derived within chiral effective field theory.

The paper is organized as follows. First, we introduce the $0\nu\beta\beta$ transition potentials in Sec. II. Section III describes the many-body methods, while Sec. IV presents our NME results. Finally, Sec. V summarizes our main conclusions and future perspectives.

II. $0\nu\beta\beta$ TRANSITION POTENTIALS

Under the closure approximation [52,53], the $0\nu\beta\beta$ NME between the initial and final nuclear states $|\Psi_i\rangle$ and $|\Psi_f\rangle$ reads

$$M^{0\nu} = \langle \Psi_f | O^{0\nu} | \Psi_i \rangle. \tag{1}$$

SM and QRPA results obtained using this approximation differ by less than 10% with respect to those including intermediate states explicitly [52–55]. This small error is consistent with the effective field theory analysis of Ref. [56]. We focus on the light Majorana neutrino exchange. For this mechanism the long-range transition operator can be cast as a sum of Fermi (F), Gamow-Teller (GT), and tensor (T) contributions $O_L^{0\nu} = O_F^{0\nu} + O_{GT}^{0\nu} + O_T^{0\nu}$, where

$$\begin{aligned} O_F^{0\nu} &= (4\pi R_A) \sum_{a\neq b} V_F^{0\nu}(r_{ab}) \tau_a^+ \tau_b^+, \\ O_{GT}^{0\nu} &= (4\pi R_A) \sum_{a\neq b} V_{GT}^{0\nu}(r_{ab})\, \sigma_{ab}\, \tau_a^+ \tau_b^+, \\ O_T^{0\nu} &= (4\pi R_A) \sum_{a\neq b} V_T^{0\nu}(r_{ab}) S_{ab}\, \tau_a^+ \tau_b^+. \end{aligned} \tag{2}$$

Here τ_a^+ is the nucleon isospin raising operator, $\boldsymbol{\sigma}_a$ represents the nucleon spin operator, $\sigma_{ab} = \boldsymbol{\sigma}_a \cdot \boldsymbol{\sigma}_b$, and the tensor operator is $S_{ab} = 3(\boldsymbol{\sigma}_a \cdot \hat{r}_{ab})(\boldsymbol{\sigma}_b \cdot \hat{r}_{ab}) - \sigma_{ab}$ with r_{ab} being the internucleon distance. The nuclear radius $R_A = 1.2\, A^{1/3}$ fm is inserted by convention to make the NME dimensionless. The coordinate-space neutrino potentials above are obtained from the standard Fourier transform:

$$V_\alpha^{0\nu}(r_{ab}) = \frac{1}{g_A^2} \int \frac{d^3\mathbf{q}}{(2\pi)^3} e^{i\mathbf{q}\cdot\mathbf{r}_{ab}} V_\alpha^{0\nu}(\mathbf{q}^2), \tag{3}$$

where $\mathbf{q}$ is the momentum transfer, α indicates F, GT, or T, and we take $g_A = 1.27$ for the axial-vector coupling.

Defining $V_\alpha^{0\nu}(\mathbf{q}^2) = \frac{1}{\mathbf{q}^2} v_\alpha(\mathbf{q}^2)$ the relevant functions can be given in terms of the nucleon isovector vector, axial, induced pseudoscalar, and magnetic form factors [28,43]:

$$\begin{aligned} v_F(\mathbf{q}^2) &= -g_V^2(\mathbf{q}^2), \\ v_{GT}(\mathbf{q}^2) &= g_A^2(\mathbf{q}^2) + \frac{2}{3}\frac{\mathbf{q}^2}{2m_N} g_A(\mathbf{q}^2) g_P(\mathbf{q}^2) \\ &\quad + \frac{1}{3}\frac{\mathbf{q}^4}{4m_N^2} g_P^2(\mathbf{q}^2) + \frac{2}{3}\frac{\mathbf{q}^2}{4m_N^2} g_M^2(\mathbf{q}^2), \\ v_T(\mathbf{q}^2) &= -\frac{2}{3}\frac{\mathbf{q}^2}{2m_N} g_A(\mathbf{q}^2) g_P(\mathbf{q}^2) - \frac{1}{3}\frac{\mathbf{q}^4}{4m_N^2} g_P^2(\mathbf{q}^2) \end{aligned}$$

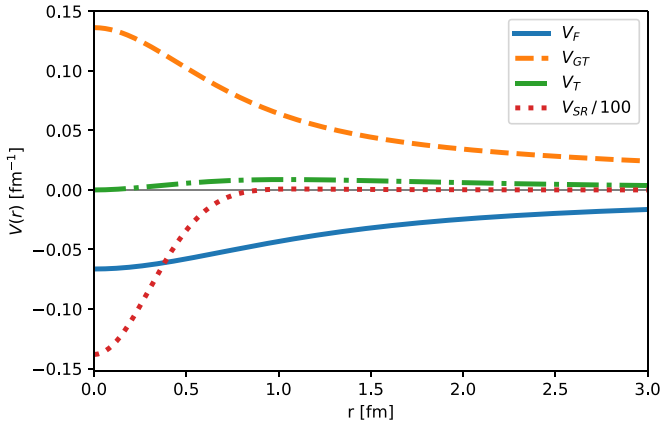

FIG. 1. Fermi (solid blue curve), Gamow-Teller (dashed orange curve), tensor (dot-dashed green curve), and short-range (dot red curve) transition potentials.

$$+\frac{1}{3}\frac{\mathbf{q}^2}{4m_N^2}g_M^2(\mathbf{q}^2), \tag{4}$$

where $m_N = 938.9$ MeV is the nucleon mass. Consistent with the $0\nu\beta\beta$ literature, for the single-nucleon form factors we adopt the simple dipole parametrization:

$$\begin{aligned} g_V(\mathbf{q}^2) &= \frac{g_V}{(1+\mathbf{q}^2/\Lambda_V^2)^2}, \\ g_M(\mathbf{q}^2) &= (1+\kappa_1)g_V(\mathbf{q}^2), \\ g_A(\mathbf{q}^2) &= \frac{g_A}{(1+\mathbf{q}^2/\Lambda_A^2)^2}, \\ g_P(\mathbf{q}^2) &= -\frac{2m_N}{q^2+m_\pi^2}g_A(\mathbf{q}^2), \end{aligned} \tag{5}$$

with vector coupling $g_V = 1$, anomalous nucleon isovector magnetic moment $\kappa_1 = 3.7$, and pion mass $m_\pi = 138$ MeV. The cutoff values are $\Lambda_V = 0.85$ GeV and $\Lambda_A = 1.04$ GeV. More sophisticated functional forms for these form factors exist [57], including some based on a systematic z expansion [58]. However, for the relatively small momentum transfer at play in $0\nu\beta\beta$ processes, $|\mathbf{q}| \approx 200$ MeV, no significant differences are expected with respect to the simple dipole ansatz.

Figure 1 displays the radial dependence of the transition potentials and shows that the T component is clearly much smaller than both the F and GT ones. This behavior is reflected in the magnitude of the corresponding NMEs, as highlighted in a number of previous calculations [15,59,60]. Including the form factors regularizes the potentials at short interparticle distances, while the typical $1/r_{ab}$ behavior at large r_{ab} is preserved.

The authors of Ref. [40] have demonstrated that an effective field theory approach of the light-neutrino exchange $0\nu\beta\beta$ decay requires a leading-order counter-term to absorb the divergences induced by the long-range neutrino potential and ensure renormalizability. This new short-range (SR) operator is associated with a Fermi spin structure and a SR neutrino potential:

$$O_S^{0\nu} = (4\pi R_A)\sum_{a\neq b} V_S^{0\nu}(r_{ab})\tau_a^+\tau_b^+, \tag{6}$$

$$V_S^{0\nu}(r_{ab}) = 2\frac{g_\nu^{NN}}{g_A^2}\delta_R^{(3)}(\mathbf{r}_{ab}), \tag{7}$$

where $\delta_R^{(3)}(\mathbf{r}_{ab})$ is a regularized three-dimensional Dirac δ function. In contrast with Ref. [41], the above definition includes a factor $1/g_A^2$ so that the full light Majorana transition operator is $O^{0\nu} = O_F^{0\nu} + O_{GT}^{0\nu} + O_T^{0\nu} + O_S^{0\nu}$. Consistent with the opposite sign in the definition of the F, GT, and T contributions, the sign of the SR potential is also different from Ref. [41]. We note that the need of introducing the SR term was shown using Eq. (1), which is obtained under the closure approximation, thereby without including intermediate states explicitly.

The value of the new coupling g_ν^{NN} arises from nonperturbative QCD dynamics and could in principle be found by matching to lattice-QCD calculations of light-neutrino exchange amplitudes [61,62]. It can also be obtained by reproducing the synthetic $2n \to 2p + 2e$ data provided by Refs. [63,64]. Alternatively, Ref. [41] notes that renormalizing the nucleon-nucleon (NN) scattering amplitude with Coulomb photon exchange also requires a short-range interaction with coupling $(C_1 + C_2)/2$, and connects $0\nu\beta\beta$ and CIB SR couplings: $g_\nu^{NN} = C_1$. Furthermore, assuming the same value for the two couplings entering the CIB of NN potentials, so that $g_\nu^{NN} \simeq (C_1 + C_2)/2$, describes well synthetic $2n \to 2p + 2e$ data [64]. We follow this approach, which allows us to evaluate short-range $0\nu\beta\beta$-decay NMEs for a variety of nuclei.

We compute the short-range behavior of nuclear states from the high-quality AV18 NN potential. Hence, when evaluating NMEs we make the consistent replacement

$$g_\nu^{NN}\delta_R^{(3)}(\mathbf{r}_{ab}) \to -\frac{6}{e^2}v_{01}^{cd}(r_{ab}) \tag{8}$$

[see Eq. (163) in Ref. [41]]. The full expression for the short-range component of the CIB term of AV18, $v_{ST}^{cd}(r_{ab})$, for the spin $S = 0$, isospin $T = 1$ channel can be found in Eq. (32) of Ref. [65] and is displayed in Fig. 1. $S = 1$ contributions are negligible at short distances. To better gauge the importance of $V_S^{0\nu}$, we also consider the expression derived from the CIB contribution of the local, Δ-full chiral effective field theory NN potential of Ref. [66]. Specifically, for the NV-Ia* model $(C_1 + C_2)/2 = -1.03$ fm^2 and $\delta_R^{(3)}(\mathbf{r}_{ab}) = e^{-r_{ab}^2/R_S^2}/(\pi^{3/2}R_S^3)$ with $R_S = 0.8$ fm.

Throughout this work, two-body transition densities play a crucial role [41,67]

$$\begin{aligned} 4\pi r^2\rho_F(r) &= \langle\Psi_f|\sum_{a<b}\delta(r-r_{ab})\tau_a^+\tau_b^+|\Psi_i\rangle, \\ 4\pi r^2\rho_{GT}(r) &= \langle\Psi_f|\sum_{a<b}\delta(r-r_{ab})\sigma_{ab}\tau_a^+\tau_b^+|\Psi_i\rangle, \\ 4\pi r^2\rho_T(r) &= \langle\Psi_f|\sum_{a<b}\delta(r-r_{ab})S_{ab}\tau_a^+\tau_b^+|\Psi_i\rangle, \end{aligned} \tag{9}$$

and $\rho_S(r) = \rho_F(r)$. All NMEs can be obtained integrating the above densities [41,67]:

$$M_\alpha^{0\nu} = \int_0^\infty dr C_\alpha^{0\nu}(r), \tag{10}$$

where we define $C_\alpha^{0\nu}(r) \equiv (8\pi R_A)4\pi r^2 \rho_\alpha(r) V_\alpha^{0\nu}(r)$ with the additional factor two to compensate the restricted sum $a < b$ in Eq. (9).

III. MANY-BODY METHODS

A. Variational Monte Carlo

The VMC method solves the Schrödinger equation by approximating the true ground state of the system with a suitably parametrized variational wave function Ψ_T. The Rayleigh-Ritz variational principle

$$\frac{\langle \Psi_T | H | \Psi_T \rangle}{\langle \Psi_T | \Psi_T \rangle} = E_T \geqslant E_0 \tag{11}$$

is exploited to find the optimal set of variational parameters. The VMC takes as input the Hamiltonian

$$H = \sum_i -\frac{\hbar^2}{2m}\nabla_i^2 + \sum_{i<j} v_{ij} + \sum_{i<j<k} V_{ijk}, \tag{12}$$

which consists of nonrelativistic single-nucleon kinetic-energy terms, and two- and three-nucleon potentials. As for the latter, in this work, we utilize the AV18 *NN* interaction [65] in combination with the UX three-nucleon ($3N$) force. UX is intermediate between the Urbana and Illinois families of potentials [38] and is essentially a truncation of the Illinois-7 (IL7) model [68]; it has the form of Eq. (17) in Ref. [38], including two-pion S- and P-wave terms and a short-range isospin-independent repulsion, with the parameter values of IL7 but without the three-pion-ring term or short-range isospin dependence. The highly successful Green's Function Monte Carlo calculations of light nuclei with AV18 + IL7 shown in Ref. [38] start from VMC calculations with AV18 + UX.

The VMC trial wave function is typically written as

$$|\Psi_T\rangle = \left(1 + \sum_{i<j<k} F_{ijk}\right)\left(\mathcal{S}\prod_{i<j} F_{ij}\right)|\Phi_J\rangle, \tag{13}$$

where F_{ij} and F_{ijk} are two- and three-body operator correlations, respectively and $\mathcal{S}$ denotes a symmetrized product over nucleon pairs. The latter is required for the wave function to be antisymmetric because, in general, the spin-isospin-dependent correlation operators F_{ij} do not commute. The F_{ij} are designed to reflect the spin-isospin and tensor dependence of the *NN* interaction, while the F_{ijk} does the same for the $3N$ force.

To account for the alpha-cluster structure of light nuclei the antisymmetric Jastrow wave function is constructed as a sum over independent-particle terms, Φ_A, each having four nucleons in an α-like core and the remaining $(A-4)$ nucleons in p-shell orbitals [69]:

$$|\Phi_J\rangle = \mathcal{A}\Bigg[\prod_{i<j<k} f_{ijk}^c \prod_{i<j\leqslant 4} f_{ss}(r_{ij}) \prod_{k\leqslant 4<l\leqslant A} f_{sp}(r_{kl}) \times \sum_{LS[n]} \Bigg(\beta_{LS[n]} \prod_{4<l<m\leqslant A} f_{pp}^{[n]}(r_{lm}) \times |\Phi_A(LS[n]JJ_zT_z)_{1234:5\ldots A}\rangle\Bigg)\Bigg]. \tag{14}$$

TABLE I. Normalized amplitudes for different spatial symmetry components in the VMC wave functions for ^{12}Be and ^{12}C.

	$^1S_0[44]$	$^3P_0[431]$	$^1S_0[422]$	$^5D_0[422]$	$^3P_0[332]$
^{12}Be			0.983		0.186
^{12}C	0.947	0.314	0.055	0.015	0.033

The operator $\mathcal{A}$ denotes an antisymmetric sum over all possible partitions of the A particles into four s-shell and $(A-4)$ p-shell states. The independent-particle wave function $|\Phi_A(LS[n]JJ_zT_z)_{1234:5\ldots A}\rangle$ with the desired total angular momentum and projection JJ_z values of a given nuclear state is obtained using orbital-spin LS coupling, which is most efficient for nuclei with up to $A \leqslant 12$. It includes a product over single-particle functions $\phi_p^{LS}(R_{\alpha l})$ $(4 < l \leqslant A)$ which are p-wave solutions of a particle in an effective α-N potential with Woods-Saxon and Coulomb terms. The symbol $[n]$ is the Young pattern that indicates the spatial symmetry of the angular-momentum coupling of the p-shell nucleons [70]. The pair correlation function for particles within the s shell, f_{ss}, arises from the structure of the α particle. The f_{sp} is similar to the f_{ss} at short range, but it has a long-range tail that approaches a constant at large distances, allowing the wave function to develop a cluster structure, i.e., the asymptotic binding is provided only by the $\phi_p^{LS}(R_{\alpha l})$. Finally, f_{pp} is set to give the appropriate clustering outside the α core, while f_{ijk}^c is a three-body central correlation induced by the *NN* potential.

For the $A = 6$ case the ^{6}He wave function has two spatial symmetry components: $^1S_0[2]$ and $^3P_0[11]$, which give a complete p-shell representation. Since ^{6}Be is taken as the charge-symmetric mirror, the $^6\text{He} \to {}^6\text{Be}$ transition densities are large and have no nodal structure. For the $A = 12$ case, a complete p-shell representation gives the ^{12}Be wave function two spatial symmetry components: $^1S_0[422]$ and $^3P_0[332]$, while ^{12}C has three additional components, given in Table I. The normalized amplitudes for each component in Table I indicate that the dominant states in the initial wave function are a very small part of the final wave function, making the $^{12}\text{Be} \to {}^{12}\text{C}$ transition densities much smaller than for $A = 6$. They are further reduced by the presence of a node in the transition densities, required by the isospin orthogonality of the two wave functions.

In an earlier comparison of VMC and SM calculations [51] the VMC wave function for ^{12}C included only the leading [44] and [431] components. While these are by far the dominant part of the final-state wave function, the small [422] and [332] components included here have a much greater spatial overlap with the ^{12}Be wave function, leading to a significant change, particularly at long range, in the transition densities. In particular, the GT NME with the more complete ^{12}C wave function is about double that of the previous VMC calculation, while

the F and T NMEs increase by 10%–20%. This improves the agreement between VMC and the earlier SM calculations of Ref. [51].

The expectation values of quantum-mechanical operators of the form of Eq. (11) contain multidimensional integrals over all nucleon positions

$$\frac{\langle\Psi_T|\mathcal{O}|\Psi_T\rangle}{\langle\Psi_T|\Psi_T\rangle} = \frac{\int d\mathbf{R}\Psi_T^\dagger(\mathbf{R})\mathcal{O}\Psi_T(\mathbf{R})}{\int d\mathbf{R}\Psi_T^\dagger(\mathbf{R})\Psi_T(\mathbf{R})}, \tag{15}$$

and Metropolis-Hastings Monte Carlo techniques are employed to efficiently evaluate them. These Monte Carlo samples are also used to compute the two-body transition densities of Eq. (9) and to estimate their statistical uncertainties.

B. Nuclear shell model

The nuclear SM is one the most successful nuclear many-body methods for describing the properties of ground and excited states, including electromagnetic and weak transitions [25–27]. It is also one of the common methods used to compute $0\nu\beta\beta$-decay NMEs [15–18].

To handle both light and heavy nuclei, the nuclear SM simplifies the many-body problem by restricting to a relatively small configuration space consisting of one or two harmonic-oscillator shells. This excludes from the calculation the core—filled with nucleons—below and the high-energy orbitals—empty—above the configuration space, but their impact is captured by an effective interaction corresponding to the configuration space. The resulting many-body Schrödinger equation is

$$H_{\rm eff}|\Psi_{\rm SM}\rangle = E|\Psi_{\rm SM}\rangle, \tag{16}$$

which we solve using the J-coupled code NATHAN [25]. Even though *ab initio* approaches allow one to obtain effective interactions solely based on NN and $3N$ forces [71], in this work we use high-quality interactions obtained from NN potentials complemented with small phenomenological adjustments, mostly on the monopole part [25].

For light $A \leqslant 12$ nuclei we use the p- and sd-shell configuration space and the PSDMWK interaction [72,73] corrected for center-of-mass contamination. In heavier nuclei we use the same configuration space and SM interactions as in previous SM studies [15,16,74]: the pf-shell with the KB3G [75] and GXPF1B [76] interactions for ^{48}Ca, the $1p_{3/2}$, $1p_{1/2}$, $0f_{5/2}$, $0g_{9/2}$ space with the GCN2850 [15], JUN45 [77], and JJ4BB [78] interactions for ^{76}Ge, and the $1d_{5/2}$, $2s_{1/2}$, $1d_{3/2}$, $0g_{7/2}$, $0h_{11/2}$ space with the GCN5082 interaction [79] for ^{130}Te and ^{136}Xe.

All the SM interactions used are isospin symmetric, while the spin-isospin symmetry relevant for GT transitions is broken due to the spin-orbit interaction and the different isovector and isoscalar pairing strengths [80]. The SM configuration space for light nuclei and ^{48}Ca include all relevant spin-orbit partner orbitals. In contrast, these are not always included in the configuration spaces in heavier nuclei. A consequence of this is that β and $2\nu\beta\beta$ matrix elements tend to be more overestimated when some spin-orbit partners are missing than when they are all included [81]. While this could also have implications for $0\nu\beta\beta$-decay NMEs, the situation is less clear [82–84].

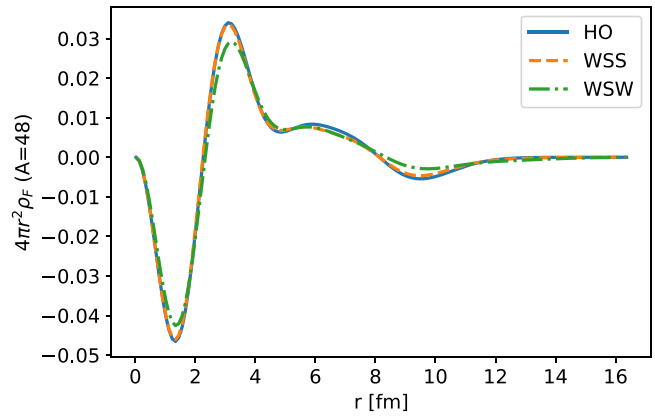

FIG. 2. Fermi transition density for $A = 48$ using the SM with HO, WSS, and WSW single-particle orbitals and the KB3G interaction.

The SM wave functions from Eq. (16) directly provide energies and other observables not dependent on radial degrees of freedom. However, for $0\nu\beta\beta$ decay the spatial part is relevant as well, and usually a harmonic oscillator (HO) basis is used for single-particle states [15,74]. Here we follow the improved approach of Ref. [51] and obtain our transition densities replacing the standard HO spatial single-particle states by Woods-Saxon (WS) ones, which reflect a more realistic long-range asymptotic behavior. We consider two kinds of WS potential: first, the standard parametrization from Suhonen (WSS) [85]; second, the potential proposed by Ref. [51] adjusted to the experimental neutron and proton separation energies and taking all orbitals in the configuration space as bound (WSW)—however, these conditions cannot be met for $A = 6$, which we only study with WSS. We have checked that alternative WS parametrizations [86] give very similar results to WSS.

In light nuclei, Ref. [51] shows that SM results with WSW orbitals greatly improve the agreement with VMC ones. The improvement with WSS is similar. However, extending the SM results with WS single-particle orbitals to heavy nuclei is challenging, and only HO calculations are currently feasible. Fortunately, we have tested in $A = 48$ that the differences between using HO and WS orbitals become smaller for heavier systems. Figure 2 shows minor differences between the F transition density computed employing the two different parametrizations of the WS orbitals and the HO one for single-particle orbitals. Likewise, the GT and T transition densities are also very similar.

Since the nuclear SM deals with regularized effective interactions, part of the short-range dynamics is missing in the wave functions. This shortcoming is common to other non *ab initio* approaches such as the QRPA, energy density functional theory and interacting boson model. Because the short-range dynamics can impact $0\nu\beta\beta$ decay NMEs, typically calculations correct for missing SRCs via a Jastrow-type function. Different parametrizations have been provided by Miller-Spencer [48] or based on Argonne and CD-Bonn

potentials [49], or by others [50,87,88]. However, in this work we do not include any additional correlations of this kind, as we introduce the correct short-range dynamics captured by the VMC calculations using the GCF.

C. Generalized contact formalism

The GCF is an effective theory for describing the impact of SRCs on a variety of nuclear distributions and observables. This formalism has proven extremely successful in modeling the short-range and high-momentum parts of different nuclear densities [45–47], and also large momentum transfer electron-scattering experiments sensitive to SRCs [89–93] and other reactions [44,94–96]. In a high-resolution picture, when two or more particles are close to each other, and, therefore, strongly interacting, the SM solution for the wave function—based on a regularized potential—becomes inaccurate [97]. For example, SRCs lead to a significant occupation of high-momentum states absent in the SM. On the other hand, QMC methods fully capture these features but are limited to light nuclei. Therefore, the GCF provides an ideal framework to quantitatively incorporate the correct short-range behavior into shell-model calculations of heavy nuclei.

The GCF is based on scale separation, leading to wave-function factorization when two particles are very close to each other. Explicitly, any nuclear wave function $\Psi(\boldsymbol{r}_1, \boldsymbol{r}_2, \ldots, \boldsymbol{r}_A)$ is expected to obey the asymptotic form [45]

$$\Psi \xrightarrow[r_{ij}\to 0]{} \sum_{\alpha} \varphi^{\alpha}(\boldsymbol{r}_{ij}) A^{\alpha}(\boldsymbol{R}_{ij}, \{\boldsymbol{r}_k\}_{k\neq i,j}). \tag{17}$$

Here $\boldsymbol{r}_{ij} = \boldsymbol{r}_j - \boldsymbol{r}_i$ and $\boldsymbol{R}_{ij} = (\boldsymbol{r}_i + \boldsymbol{r}_j)/2$ are the relative and center-of-mass coordinates of the pair, and α denotes its quantum numbers, i.e., parity π_α, spin s_α, total angular momentum j_α, and projection $j_{\alpha z}$, and total isospin t_α and projection $t_{\alpha z}$. Isospin quantum numbers are relevant to keep the nuclear wave function Ψ antisymmetric under permutations of any two nucleons. This convention is equivalent to the one in most previous GCF studies considering wave functions antisymmetric under separate permutations of protons and neutrons. The solution of the zero-energy two-body Schrödinger equation $\varphi^{\alpha}(\boldsymbol{r}_{ij})$ describes the pair dynamics when the two nucleons are close together. It is a universal function, i.e., identical for all nuclei and all quantum states, but depends on the particular nuclear interaction. It can be written as

$$\varphi^{\alpha}(\boldsymbol{r}) \equiv \eta_{t_\alpha, t_{\alpha z}} \sum_{\ell_\alpha \in \pi_\alpha} \phi^{\alpha}(r) [Y_{\ell_\alpha}(\hat{\boldsymbol{r}}) \otimes \chi_{s_\alpha}]^{j_\alpha m_\alpha}, \tag{18}$$

where η_{t,t_z} is an isospin factor, Y_{lm} are spherical harmonics, χ_{sm} is the two-body spin function, and the sum runs over orbital angular momenta ℓ_α of correct parity π_α that can couple with s_α yielding j_α. The radial dependence is modeled by $\phi^{\alpha}(r)$, which is independent of $j_{\alpha z}$ and, to good accuracy, also of $t_{\alpha z}$ due to isospin symmetry.

Based on this asymptotic form, the nuclear *contacts* for a nucleus with A nucleons are defined as

$$C^{\alpha\beta} = \frac{A(A-1)}{2} \langle A^{\alpha} | A^{\beta} \rangle. \tag{19}$$

The factor $A(A-1)/2$ appears in place of the number of proton-proton, neutron-proton, or neutron-neutron pairs present in previous publications because here the wave function is antisymmetric under permutation of any two nucleons.

The diagonal contacts $C^{\alpha\alpha}$ are proportional to the number of correlated pairs in the nucleus with quantum numbers α. However, in this work we apply the GCF to describe the short-range behavior of the two-body densities relevant for $0\nu\beta\beta$ transitions. Hence, we define new contact parameters that involve different initial (i) and final (f) nuclear states as

$$C^{\alpha\beta}(f, i) = \frac{A(A-1)}{2} \langle A^{\alpha}(f) | A^{\beta}(i) \rangle. \tag{20}$$

Using the above definition, we can write the dominant contributions to the transition densities defined in Eq. (9) at short distances. For F and GT transitions, we expect pairs in a s-wave state, mainly with $s = 0$, $j = 0$, $t = 1$. Denoting the corresponding contact parameter for a transition of two neutrons to two protons ($nn \to pp$) with such quantum numbers as $C^0_{pp,nn}(f, i)$, the F transition density can be expressed as

$$\rho_F(r) \xrightarrow[r\to 0]{} \frac{1}{4\pi} |\phi^0(r)|^2 C^0_{pp,nn}(f, i), \tag{21}$$

where $\phi^0(r)$ is the radial function for the $\ell = 0$, $s = 0$, $j = 0$, $t = 1$ channel. Since $\rho_S = \rho_F$, the above asymptotic form is also valid for the transition density associated with the short-range operator of Eq. (7). As for the GT transition, the σ_{ab} operator leads to a factor of (-3) in this $s = 0$ channel and we similarly obtain

$$\rho_{GT}(r) \xrightarrow[r\to 0]{} -\frac{3}{4\pi} |\phi^0(r)|^2 C^0_{pp,nn}(f, i), \tag{22}$$

which implies the following relation between the F and GT densities for short distances

$$\rho_{GT}(r \lesssim 1 \text{ fm}) = -3\rho_F(r \lesssim 1 \text{ fm}). \tag{23}$$

Based on our previous experience with two-body densities [46,47], these expressions should provide a good description of the transition densities for $r \lesssim 1$ fm. The $s = 1$ contribution is negligible at short distances, but it is accounted for at larger distances using the SM calculations.

To calculate the $0\nu\beta\beta$ matrix elements, we wish to combine the GCF expressions, valid at short distances, and the long-range behavior of the nuclear SM many-body wave functions. The main unknowns in this approach are the values of the relevant contacts, which in general depend on the nucleus and on the particular nuclear interaction. Nevertheless, previous studies have shown that for the case of the contacts defined in Eq. (19), contact ratios $C^{\alpha\alpha}(X)/C^{\alpha\alpha}(Y)$, for any two nuclei X and Y, are model independent [47,96,98]. In this sense, contact ratios can be interpreted as long-range, low-resolution quantities that do not depend on the details of the nuclear interaction.

Such a model independence is expected to hold also for ratios of the contacts defined in Eq. (20). Therefore, the ratio of the contacts $C^{0,\mathrm{SM}}_{pp,nn}(f_1, i_1)/C^{0,\mathrm{SM}}_{pp,nn}(f_2, i_2)$—indices 1 and 2 denote different $0\nu\beta\beta$ decays—is inferred from SM transition densities at short distances. Then, the contact $C^{0,V_N}_{pp,nn}(f_2, i_2)$ is obtained by fitting the short-range behavior to the transition

density "2" computed with VMC for a given realistic nuclear interaction V_N. Finally, the contact for transition "1" is obtained exploiting the model independence of the ratios:

$$C^{0,V_N}_{pp,nn}(f_1,i_1) = \frac{C^{0,\mathrm{SM}}_{pp,nn}(f_1,i_1)}{C^{0,\mathrm{SM}}_{pp,nn}(f_2,i_2)} C^{0,V_N}_{pp,nn}(f_2,i_2). \quad (24)$$

This procedure allows us to obtain contact values of heavy nuclei for any nuclear interaction, using only a single *ab initio* calculation for light nuclei and SM ones for both heavy and light nuclei. In Sec. IV we demonstrate the validity of the model independence of contact ratios.

The contact value $C^{0,V_N}_{pp,nn}(f_1,i_1)$ and the corresponding short-range radial function fully determine the short-range part ($r \lesssim 1$ fm) of the transition densities for a given nuclear interaction. On the other hand, the SM is expected to provide high-quality transition densities at long distances. Thus, we merge the GCF and SM results continuously, by scaling the SM transition densities to match the GCF expression around $r \simeq 1$ fm. This approach, dubbed GCF-SM, allows us to obtain the F and GT transition densities for any given nuclear interaction—including heavy nuclei where direct *ab initio* calculations with high-resolution potentials are currently not available. We integrate the resulting transition densities as in Eq. (10) to evaluate the relevant $0\nu\beta\beta$ NMEs.

In the case of the T transitions the leading contribution is expected to come from p-wave channels. There are three such channels (with $j = 0, 1, 2$) which complicates the analysis. In addition, comparing SM and VMC calculations, it seems that the model-independence of the ratios does not hold for the T case. For this reason, in this work we estimate the T matrix element by the SM results with a 50% uncertainty. This should not have a big impact on the total NME as the T part is expected to be small compared with the GT contribution [15,28].

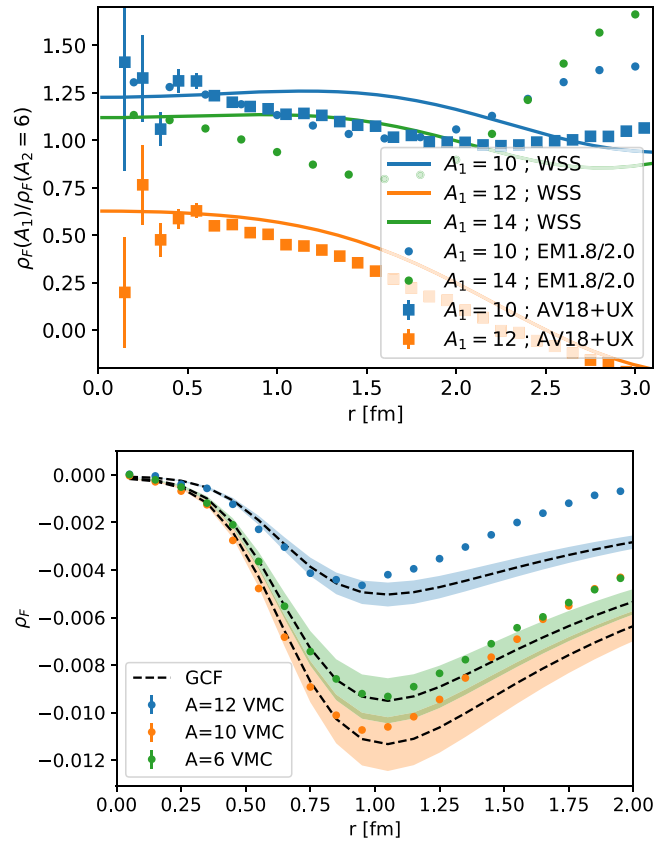

FIG. 3. (top) Fermi transition density ratio for different nuclei, calculated using different interactions (AV18 + UX, EM1.8/2.0, and SM). The EM1.8/2.0 results are IT-NCSM calculations from Ref. [99]. (bottom) VMC Fermi transition densities (solid circles) compared with the GCF description using the universal function squared and fitted value of the contact (dashed black lines and bands).

IV. RESULTS AND DISCUSSION

A. Light nuclei

To use the GCF to describe the short-range part of the transition densities, we evaluate the contact $C^0_{pp,nn}(f,i)$ assuming the model independence of contact ratios. In light nuclei, the availability of both VMC and SM $0\nu\beta\beta$ transition densities allows us to test the accuracy of this approach. Figure 3 (top panel) displays three ratios of F transition densities: ^{12}Be $\to$ ^{12}C decay, ^{10}Be $\to$ ^{10}C decay, and ^{14}C $\to$ ^{14}O decay, all relative to ^{6}He $\to$ ^{6}Be decay. These have been obtained with the VMC method for the AV18 + UX interaction and with the SM method for the PSDMWK interaction, together with the importance-truncated no-core shell model (IT-NCSM) calculations of Ref. [99] in which the chiral EM1.8/2.0 interaction was used ($A = 14$ calculations are not available for the VMC method, while $A = 12$ calculations are not available for the IT-NCSM method.) Based on Eq. (21), we expect these ratios to reach a plateau at short distances, representing the contact ratio of the two transitions. Indeed, the SM calculations show such a clear plateau. The EM1.8/2.0 ratios seem to also reach a plateau for $r \lesssim 0.5$ fm. The AV18 + UX ratio are somewhat noisy at the very short distances ($r \lesssim 0.5$ fm), but focusing on the 0.5 fm $\lesssim r \lesssim$ 1 fm range, we also observe a plateau. In addition, we can see that for all cases separately (i.e., $A = 10$, $A = 12$, and $A = 14$) the value of the ratio at short distances is very similar for the different interactions, indicating model independence. Note that model independence is also observed when considering similar ratios of heavier nuclei using different SM interactions.

To corroborate the fact that AV18 + UX VMC calculations for different nuclei are indeed characterized by a universal behavior at short distances, we show in Fig. 3 (bottom panel) the VMC Fermi transition densities compared with the GCF universal function squared (calculated using the AV18 interaction). The contact value has been fit so as to reproduce the VMC results at $r < 1.0$ fm based on Eq. (21), while the error bands are obtained by changing the best-fit value by $\pm 10\%$. It clearly emerges that at short distances, the VMC transition densities are well described by the same universal function for $r < 1$ fm, as predicted by the GCF.

To gauge the accuracy of our approach, we use the VMC transitions for $A = 6$ and $A = 10$ to predict results for $A = 12$. The contact $C^0_{pp,nn}(^{10}\mathrm{Be}, ^{10}\mathrm{C})$ is fit to the VMC calculations using the functional form of Eq. (21). We then obtain the $A = 12$ contact $C^0_{pp,nn}(^{12}\mathrm{Be}, ^{12}\mathrm{C})$ based on the model

independence of Eq. (24), multiplying $C^0_{pp,nn}(^{10}\mathrm{Be}, ^{10}\mathrm{C})$ by the average value of the SM ratio $\rho_F(A=12)/\rho_F(A=10)$ at short distances. We repeat the same procedure using as input the VMC transition densities for $A=6$. Comparing the two approaches yields $\lesssim$10% differences in the extracted contact values, and we take the average as our best estimate for $C^0_{pp,nn}(^{12}\mathrm{Be}, ^{12}\mathrm{C})$, associated with a $\pm$10% uncertainty.

Once the value of the contact is determined, we construct the short-range part of the F, GT, and SR transition densities with Eqs. (21) and (22). To highlight the consistency of the approach, we note that the value of the contact is extracted from VMC calculations using the AV18 + UX Hamiltonian, and the two-body function $\phi^0(r)$ is computed with the same AV18 *NN* force.

For long distances we use the SM transition densities, after rescaling them so that they are continuously merged with the short-range part. This part is expected to be well described by the SM, given the very good description it gives of nuclear structure and spectroscopy [25,26]. In particular, long-range correlations have been studied extensively in $0\nu\beta\beta$ studies [100–102], and the SM has proven to capture well important correlations such as those related to high-seniority components [103] or proton-neutron pairing [80]. Furthermore, a recent statistical analysis for ^{48}Ca suggests that the lowest-energy 2^+ state in ^{48}Ti and especially the $2\nu\beta\beta$ NME are the nuclear properties better correlated with the $0\nu\beta\beta$ NME [104]. These two observables are well described by SM calculations, in the case of the $2\nu\beta\beta$ matrix after accounting for a "quenching" factor common to β decays and which is the same for all nuclei in the same mass region [32,105,106]. In sum, even though it is possible that $0\nu\beta\beta$ NMEs could be sensitive to different physics than other nuclear properties, we expect that the GCF-SM describes also well the long-range part of the transition densities.

The upper, middle, and lower panels of Fig. 4 display the F, GT, and SR transition densities obtained with the above procedure. The band is obtained by randomly varying separately the contact value within its $\pm$10% uncertainty, and the matching point of GCF and SM between 0.8–1.0 fm. Figure 4 shows an overall good agreement between the GCF-SM and the VMC results. In particular, our new method greatly improves upon the short-range behavior of the SM transitions densities, bringing them into excellent agreement with the VMC ones. It has to be noted that while introducing ad hoc Jastrow-like correlations into SM calculations certainly ameliorates their short-range behavior, the agreement with *ab initio* results is not as good [51]. In addition, the GCF can readily accommodate different interactions and correct SM calculations in a consistent fashion. The long-range part of the transitions ($r \gtrsim 1$ fm), taken from the SM, also agrees with the VMC, although some small differences can be observed for the F and GT transitions. In this regard, an important role is played by the complete *p*-shell representation of the VMC ^{12}C wave function utilized in this work, in contrast with earlier VMC calculations [41,43,51] that only included the leading [44] and [431] spatial symmetry components. As expected, the transition density of the SR operator is almost perfectly described by our approach, at both short and long distances.

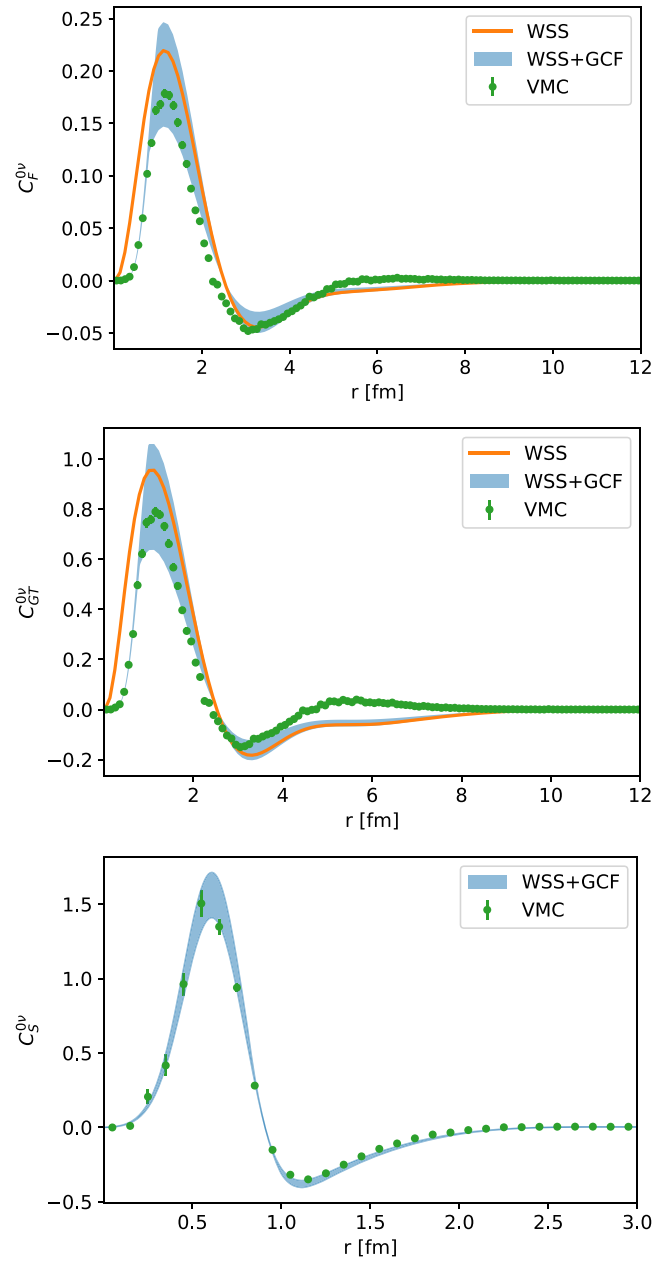

FIG. 4. Fermi, Gamow-Teller, and short-range transition densities for the $^{12}\mathrm{Be} \to {}^{12}\mathrm{C}$ decay calculated with the SM WSS (orange line), VMC (green points), and the combination of the GCF and SM WSS (blue band) approaches. For the latter, only VMC calculations for $A=6$ and $A=10$ are used to extract the $^{12}\mathrm{Be} \to {}^{12}\mathrm{C}$ contact value.

We further gauge the accuracy of the GCF-SM method by using either both the $A=10$ and $A=12$, or the $A=6$ and $A=12$ VMC transition densities, to predict the $A=6$ or $A=10$ ones, respectively. The latter are then integrated as in Eq. (10) to obtain the corresponding NMEs $M^{0\nu}_\alpha$. Figure 5 compares the GCF-SM $A=6$, $A=10$, and $A=12$ F (upper panel), GT (middle panel), and SR (lower panel) NMEs for these nuclei to the VMC and standard SM results—see Table II for their numerical values. Most of the VMC and GCF-SM matrix elements are consistent within the error

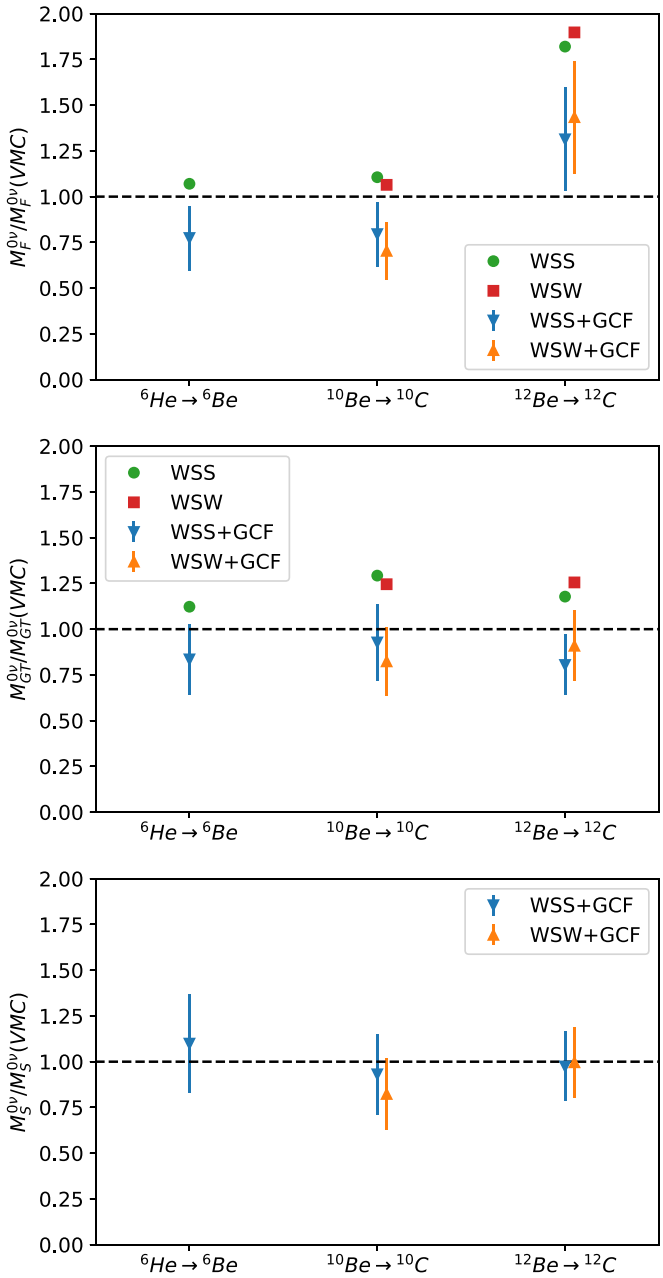

FIG. 5. Ratio of nuclear matrix elements of the F (upper panel), GT (central panel), and SR (lower panel) operators. Results obtained combining the GCF and SM, or just the SM approach, divided by the VMC ones with the AV18 + UX Hamiltonian. Both WSS and WSW parametrizations are used for the SM calculations.

bars—little dependence on the particular WS parametrization is observed—and SR NMEs agree especially well. The SR SM values without correcting for SRCs, not shown in Fig. 5, are about 10 times larger than the VMC ones due to the scale of the AV18 SR potential, see Fig. 1. While a rigorous uncertainty quantification of SM results is difficult to carry out, the GCF-SM error estimation appears to be reasonable, although it does not include directly all possible error sources.

We note that using SR transition potential from the NV-Ia* interaction changes the value of $M_S^{0\nu}$ by less than 20%, despite the differences in the shape of the transition densities $C_S^{0\nu}(r)$ being more dramatic. Nonetheless, fully consistent calculations of SR operators for potentials other than AV18 require using the appropriate two-body function $\phi^0(r)$ and the corresponding VMC transition densities. This is left for future work.

Finally, we have studied the effect of $3N$ forces on the $A = 6$ VMC NME values. Adding the $3N$ force increases the binding energy and makes the nucleus more compact. The F and GT matrix elements to the mirror nucleus change by less than $\pm 1.5\%$. However, the small tensor is increased by 15%. This is probably because the $3N$ force boosts the fraction of the wave function with $S \geqslant 1$ from 19% to 24%.

TABLE II. Fermi, Gamow-Teller, and short-range NMEs for the ^{6}He $\to$ ^{6}Be, ^{10}Be $\to$ ^{10}C and ^{12}Be $\to$ ^{12}C transitions calculated using different methods. VMC_2 stands for VMC calculations with two components for ^{12}C, while VMC_5 includes five components. The latter is used to extract the contact ratios.

Transition	Method	F	GT	SR
^{6}He $\to$ ^{6}Be	VMC	0.935	3.706	0.296
	WSS	1.001	4.160	3.293
	WSS + GCF	0.72(16)	3.08(71)	0.32(8)
^{10}Be $\to$ ^{10}C	VMC	1.178	3.632	0.528
	WSW	1.254	4.524	4.631
	WSS	1.303	4.695	4.834
	WSW + GCF	0.83(19)	2.99(66)	0.43(10)
	WSS + GCF	0.93(20)	3.36(76)	0.50(12)
^{12}Be $\to$ ^{12}C	VMC_2	0.102	0.365	0.347
	VMC_5	0.111	0.751	0.371
	WSW	0.211	0.943	2.677
	WSS	0.203	0.885	2.680
	WSW + GCF	0.16(4)	0.69(14)	0.37(7)
	WSS + GCF	0.15(3)	0.61(12)	0.36(7)

B. Heavy nuclei

Having validated the accuracy of the GCF-SM approach on light nuclei, we now turn our analysis to nuclei relevant to the $0\nu\beta\beta$ decay experimental program, currently beyond the reach of the VMC method. We obtain GCF-SM predictions of $0\nu\beta\beta$ transitions analogously to light nuclei, the only difference being that we use all the VMC and SM transition densities for $A = 6$, $A = 10$, and $A = 12$ nuclei to extract the contact values. The short-range components of the transition densities are modeled according to Eqs. (21) and (22) and continuously matched to rescaled SM results, so that the long-range part $C_\alpha^{0\nu}(r)$ is fully specified.

We note that the experimentally relevant decays are isospin-changing transitions ($\Delta T = 2$). Nevertheless, we use also isospin-conserving ($\Delta T = 0$) transitions of light nuclei ($A = 6$ and $A = 10$) to calculate contact values because the GCF model-independence of contact ratios does not distinguish between isospin-conserving and isospin-changing decays. The validity of this statement was tested above for the $A = 12$, $\Delta T = 2$ transition.

TABLE III. Fermi, Gamow-Teller, and short-range NMEs for the ^{48}Ca → ^{48}Ti, ^{76}Ge → ^{76}Se, ^{130}Te → ^{130}Xe, and ^{136}Xe → ^{136}Ba transitions using the SM (HO, WSS, WSW) and the GCF-SM with different WS orbitals to fix the values of the contact ratios. The KB3G SM interaction was used for $A = 48$, GCN2850 was used for $A = 76$, and GCN5082 for $A = 130$ and $A = 136$. Results using additional SM interactions appear in Appendix A.

Transition	Method	F	GT	SR
^{48}Ca → ^{48}Ti	WSS	0.144	0.893	2.389
	WSW	0.138	0.868	2.110
	HO	0.145	0.906	2.388
	WSS + GCF	0.09(2)	0.60(12)	0.32(6)
	WSW + GCF	0.09(2)	0.57(12)	0.28(5)
	HO(S) + GCF	0.09(2)	0.61(13)	0.32(6)
	HO(W) + GCF	0.09(2)	0.60(12)	0.32(6)
^{76}Ge → ^{76}Se	HO	0.357	3.030	5.346
	HO(S) + GCF	0.23(5)	2.14(47)	0.70(13)
	HO(W) + GCF	0.23(5)	2.12(48)	0.69(13)
^{130}Te → ^{130}Xe	HO	0.418	2.882	5.942
	HO(S) + GCF	0.27(6)	2.02(44)	0.78(15)
	HO(W) + GCF	0.27(6)	1.97(43)	0.77(15)
^{136}Xe → ^{136}Ba	HO	0.335	2.312	4.725
	HO(S) + GCF	0.22(5)	1.61(36)	0.62(12)
	HO(W) + GCF	0.22(4)	1.60(36)	0.61(12)

While for light nuclei $A \leqslant 12$ WSS and WSW clearly improve the transition densities in Eq. (9) in relation with the VMC results, the HO and WS radial wave functions lead to very similar results in ^{48}Ca, see Fig. 2. Based on this observation, for $A \geqslant 48$ nuclei our SM transitions are obtained with HO orbitals. On the other hand, the SM transition densities for $A = 6$, $A = 10$, and $A = 12$ used to extract the contact ratios against AV18 + UX VMC results are always carried out with WS single-particle states. Specifically, we denote the HO results for heavy nuclei "HO(S)" or "HO(W)" depending on whether the WSS or WSW parametrization is used to extract the contacts from light-nuclei transitions.

Figure 6 illustrates the differences between SM and GCF-SM transition densities for the ^{76}Ge → ^{76}Se decay, covering the F, GT, and SR operators. The short-range behavior of the SM is modified in a consistent fashion as in light nuclei and reflects the underlying realistic nuclear potential. Analogously to Fig. 5, we do not report the SM transition densities for the SR operator, as the corresponding NMEs are about seven times larger than the GCF-SM values.

The GCF-SM results for the F, GT, and SR matrix elements for $A = 48$, $A = 76$, $A = 130$, and $A = 136$ are displayed in Fig. 7 and their numerical values are listed in Table III. They are compatible with NME results using alternative SM interactions given in Appendix A. We supplement these predictions with estimates for the uncertainties associated with the matching procedure and the extraction of the contact ratios as described in Sec IV A. Our results indicate that the F and GT matrix elements are reduced by about 20%–45% compared with the conventional SM calculations due to the additional SRCs introduced via the GCF.

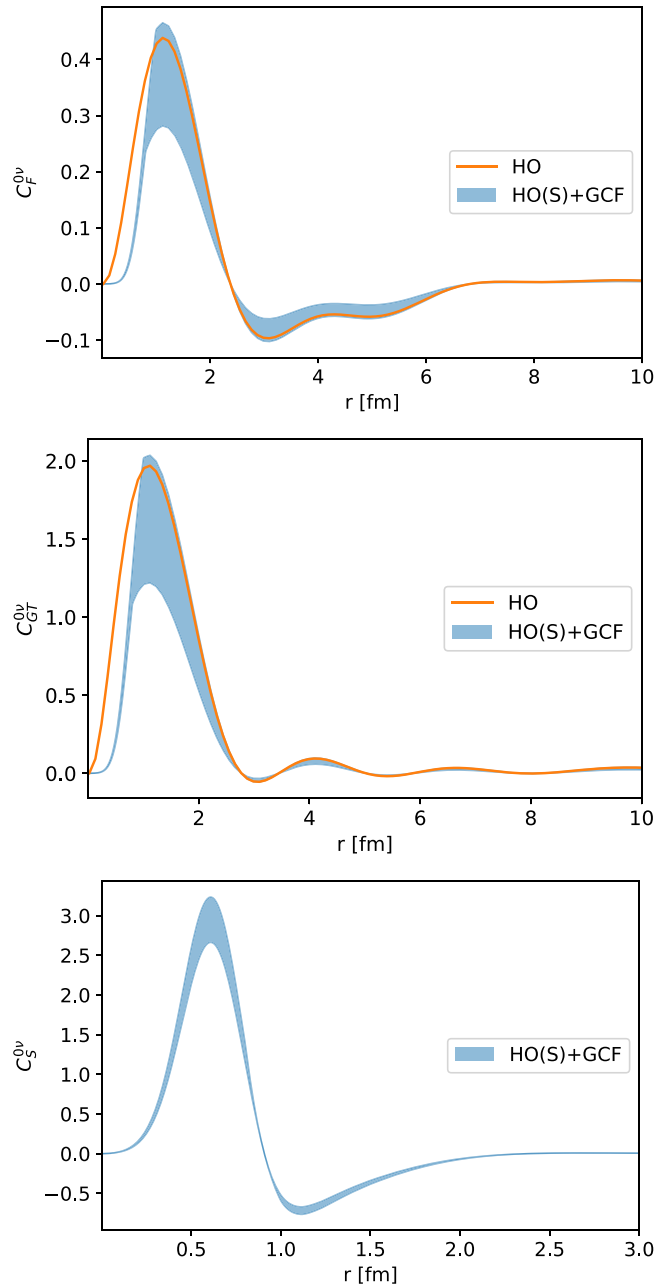

FIG. 6. Transition densities $C_F^{0\nu}$ (upper panel), $C_{GT}^{0\nu}$ (middle panel), and $C_S^{0\nu}$ (lower panel) for the ^{76}Ge → ^{76}Se decay obtained with the SM with HO orbitals (orange line) and the GCF-SM (blue band). The GCN2850 SM interaction was used.

The bottom panel of Fig. 7 shows that the value of the short-range NME is significantly smaller in $A = 48$ than in heavier nuclei, a trend which is similar when we replace the SR transition potential with the one corresponding to the NV-Ia* interaction—$M_S^{0\nu}$ only changes by about 20%. Figure 7 also indicates that our short-range NMEs are in general smaller but consistent within error bars with the SM results by Jokiniemi *et al.* [107], which cover a wider range of SR transition potentials—not including the AV18 one we use—and are further corrected by the SRC parametrization

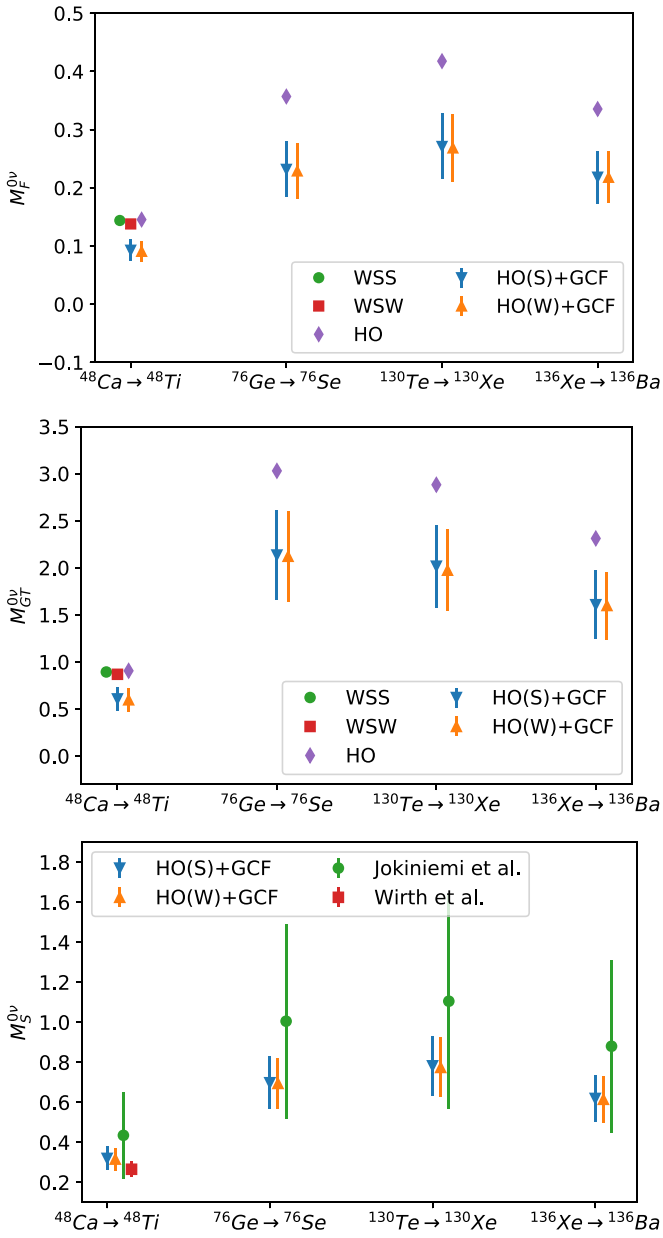

FIG. 7. NMEs of the F (upper panel), GT (middle panel), and SR (lower panel) operators using the GCF-SM and the SM approaches, compared with the SR results of Jokiniemi *et al.* [107] and Wirth *et al.* [36]. The KB3G SM interaction was used for $A = 48$, GCN2850 was used for $A = 76$, and GCN5082 for $A = 130$ and $A = 136$.

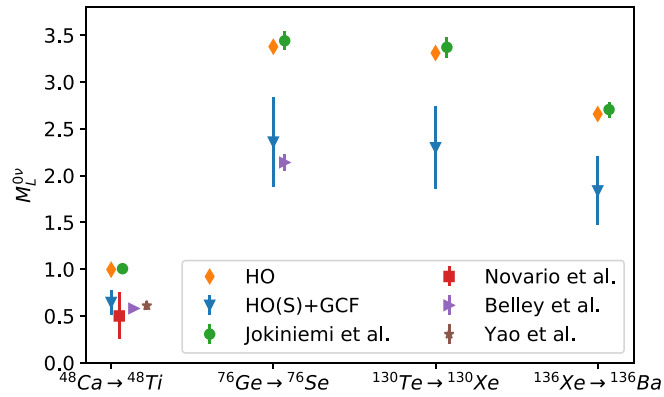

FIG. 8. Long-range matrix element $M_L^{0\nu}$ calculated with the combination of the GCF and the SM (blue), the SM without (orange) and with SRCs from Jokiniemi *et al.* (green) [107], CC theory from Novario *et al.* (red) [34], the VS-IMSRG method from Belley *et al.* (purple) [37], and the IM-GCM from Yao *et al.* (brown) [35]. For $A = 48$ we use the KB3G SM interaction, GCN2850 for $A = 76$, and GCN5082 for $A = 130$ and $A = 136$.

of Ref. [49]. In contrast, we only use one SR potential and just include uncertainties associated with the matching procedure and the extraction of the contact ratios. The $M_S^{0\nu}$ values obtained with the QRPA by Jokiniemi *et al.* are somewhat larger than ours. Remarkably, our SR NME for ^{48}Ca is in good agreement with the in-medium similarity renormalization group (IMSRG) combined with the generator coordinate method (IM-GCM) *ab initio* result of Wirth *et al.* [36]. This is particularly interesting since they use a different nuclear interaction and also a different procedure for determining the SR coupling g_ν^{NN}.

Eventually, the total $0\nu\beta\beta$ decay NME is the sum of the long-range term $M_L^{0\nu} = M_{GT}^{0\nu} + M_F^{0\nu} + M_T^{0\nu}$ and the short-range matrix element $M_S^{0\nu}$. As discussed in Sec. III, we evaluate the relatively small M_T contribution within the standard SM, associated with a conservative 50% uncertainty. Figure 8 presents our results for $M_L^{0\nu}$, highlighting that the GCF-SM reduces the value of $M_L^{0\nu}$ by about 15%–40% compared with the original SM calculations. Therefore, our approach introduces a much larger SRC effect than the one from typical SRC parametrizations such as the one from Ref. [49] used in SM $0\nu\beta\beta$ studies, see the very small difference between the SM (HO) and Jokiniemi *et al.* results from Ref. [107]. Figure 8 also compares our NMEs with the *ab initio* results of Novario *et al.* [34] using the coupled cluster (CC) method and of Yao *et al.* [35] using the IM-GCM approach for ^{48}Ca and of Belley *et al.* [37] using the valence space IMSRG (VS-IMSRG) method for ^{48}Ca and ^{76}Ge. Our long-range NMEs are in very good agreement with all the *ab initio* results for ^{48}Ca even though these calculations use different nuclear interactions, and are also consistent with the VS-IMSRG for ^{76}Ge. As our estimation of the tensor matrix element is currently based on SM calculations, it is also useful to compare our results for $M_F^{0\nu} + M_{GT}^{0\nu}$ with those of *ab initio* calculations. Belley *et al.* [37] obtain $M_F^{0\nu} + M_{GT}^{0\nu} = 0.7$ for ^{48}Ca, and $M_F^{0\nu} + M_{GT}^{0\nu} = 2.50$ for ^{76}Ge. This is in very good agreement with our results (see Table III). The good agreement with *ab initio* calculations supports our predictions for ^{130}Te and ^{136}Xe, for which *ab initio* NMEs are not available currently.

Comparing Figs. 7 and 8, it is apparent that the SR term contributes significantly to the total NME: $M_S^{0\nu}$ is around 35%–60% of $M_L^{0\nu}$ for $A = 48$—in good agreement with Ref. [36]—and around 25%–40% for the heavier nuclei. Since $M_S^{0\nu}$ has the same sign as $M_L^{0\nu}$, the total matrix element would be enhanced, also in agreement with Ref. [36]. Despite the differences between our results and the SM ones of Jokiniemi

et al., the relative importance of the SR term is overall similar, while the QRPA predicts somewhat larger ratio values [107].

It is important to highlight the differences between the GCF-SM and previous attempts to include SRCs into the SM and other approaches based on regularized interactions. Some of the correlation functions that produce larger effect of SRCs, e.g., those by Miller and Spencer [48], were criticized because they lead to violation of isospin symmetry because they yield $\int_0^\infty r^2 \rho_F(r) dr \neq 0$ even when the isospins of the initial and final states differ [108]. Given the relatively large effects of SRCs, one might think that the GCF-SM approach can suffer from the same shortcomings. Reference [108] also claims that, in order to respect isospin symmetry, correlation functions should peak around $r \simeq 1$ fm with a value above 1 to compensate for the reduction of probability at short distances. This behavior eventually leads to a relatively small effect on the NME values. In contrast, to match the VMC and SM results an appropriate correlation function should be defined as the ratio of the corresponding transition densities—by construction, multiplying the SM results by this correlation function reproduces the VMC one. By comparing the VMC and SM transition densities presented in Fig. 4, we notice that the correlation function does not peak around $r \simeq 1$ fm. Furthermore, the GCF-SM approach has a significant difference in that the SM results are rescaled to match the short-range behavior, so that the effect of the GCF does not approach unity at long distances unlike most SRC parametrizations. This rescaling allows the GCF-SM to compensate for the short-range reduction without a peak at $r \simeq 1$ fm. Some violation of the isospin orthogonality can still be found in our actual results, but this is due to subleading corrections, like three-body correlations, and possible small differences between the SM and the exact solution at long distances. For an extended discussion, see Appendix B. Eventually, the good agreement between the GCF-SM and VMC results (which rigorously obey isospin orthogonality) in light nuclei shown in Fig. 4 demonstrates the accuracy of our method.

In addition, most of the available SRC functions assume in their derivation a simple form for the uncorrelated wave function, for instance, the single Slater determinant in Ref. [49]. The latter differs from the SM wave function and therefore leads to inconsistencies when combined with SM calculations. Likewise, the correlation function based on VMC calculations introduced in Ref. [87] also uses a simple function for the uncorrelated part. Furthermore, Ref. [87] uses proton-proton VMC densities of a given nucleus in contrast to the transition densities involving the initial and final nuclei used in the GCF-SM approach. In short, the GCF-SM replaces the need of introducing SRC functions by directly providing the appropriate short-range structure for any given *NN* interaction.

V. CONCLUSIONS

We have introduced a novel protocol based on the GCF that combines SM and QMC methods to compute $0\nu\beta\beta$ decay nuclear matrix elements of heavy nuclei relevant for experimental searches. The GCF captures the short-distance behavior of transition densities computed within VMC, while rescaled SM calculations are used to model the long-range components. A key role in our GCF-SM approach is played by the "contact" values, which determine the number of short-range correlated pairs participating in the transition densities. Assuming their model-independence—extensively verified in diagonal two-body densities—we extract the contact values of heavy nuclei combining VMC calculations of light nuclei with SM transitions of both light and heavy isotopes. We verify the accuracy of this procedure on VMC transition densities of $A = 6$, $A = 10$, and $A = 12$ nuclei. The latter are also improved compared with earlier VMC calculations by introducing a complete *p*-shell representation of the ^{12}C wave function. We supplement the GCF-SM predictions by estimates of uncertainties due to the matching procedure and the extraction of the contact ratios.

We employed the GCF-SM to predict NMEs for ^{48}Ca, ^{76}Ge, ^{130}Te, and ^{136}Xe. The long-range matrix elements are appreciably reduced by 15%–40% with respect to the SM calculations. In particular, the impact of SRCs is significantly larger within the GCF-SM than when using relatively soft functions to incorporate SRCs effects into the SM. In fact, our approach replaces altogether the need of using correlation functions, since, besides an overall normalization factor, the short-range behavior of the transition density is fully determined by the GCF. Remarkably, our results are consistent within the error bars with recent *ab initio* results for ^{48}Ca and ^{76}Ge from the CC, VS-IMSRG, and IM-GCM methods. Furthermore, we make GCF-SM predictions for the heaviest emitters used in $0\nu\beta\beta$ searches: ^{130}Te and ^{136}Xe, for which *ab initio* results are not currently available. Given the agreement with the VMC in the light-nuclei sector and with other *ab initio* approaches for ^{48}Ca and ^{76}Ge, we believe that the GCF-SM is a reliable complementary approach to calculate $0\nu\beta\beta$ NMEs. This might help to reduce the overall uncertainty in the NMEs due to the different values obtained using different many-body methods.

The GCF-SM approach is especially suitable for calculating the recently introduced leading-order SR matrix element. Using a potential consistent with the AV18 interaction used to compute the transition densities at short distances, we find that the SR term enhances the total NME by 25%–40% in heavy nuclei, which is consistent with IM-GCM and SM estimations. Nonetheless, our SR NMEs obtained based on the CIB of AV18 may need to be rescaled once the correct g_ν^{NN} coupling is determined—see Ref. [63] for a recently proposed strategy using synthetic data. As we mentioned above, the choice of $g_\nu^{NN} \simeq (C_1 + C_2)/2$ describes well this synthetic data, within 35% in the case studied in Ref. [64]. This approximation is also supported by the QCD analysis in Ref. [109]. Nonetheless, since the C_i couplings are scheme and scale dependent, it is difficult to quantify the exact impact of fitting g_ν^{NN} directly to the synthetic data.

A limitation of this work is the absence of two-body currents in the $0\nu\beta\beta$ decay, which are related to a consistent treatment of the transition operator. Two-body currents are necessary to reproduce β-decay matrix elements [29,110], but are not fully included in any $0\nu\beta\beta$ calculation yet, where their impact has only been estimated within simple approximations [111–113]. However, Refs. [29,110] indicate that two-body currents are relatively less important when using hard nuclear

TABLE IV. Fermi, Gamow-Teller, and short-range NMEs for the decays ^{48}Ca → ^{48}Ti with the GXPF1B interaction and ^{76}Ge → ^{76}Se with the JJ4BB and JUN45 interactions.

Transition	Method	F	GT	SR
^{48}Ca → ^{48}Ti (GXPF1B)	WSS	0.133	0.763	2.115
	WSW	0.127	0.742	1.867
	HO	0.133	0.770	2.098
	WSS + GCF	0.08(2)	0.50(11)	0.28(5)
	WSW + GCF	0.08(2)	0.49(11)	0.24(5)
	HO(S) + GCF	0.08(2)	0.51(11)	0.28(5)
	HO(W) + GCF	0.08(2)	0.50(11)	0.27(5)
^{76}Ge → ^{76}Se (JJ4BB)	HO	0.357	3.051	4.949
	HO(S) + GCF	0.23(5)	2.16(48)	0.64(12)
	HO(W) + GCF	0.23(5)	2.13(48)	0.63(12)
^{76}Ge → ^{76}Se (JUN45)	HO	0.395	3.283	5.672
	HO(S) + GCF	0.26(5)	2.30(0.51)	0.74(14)
	HO(W) + GCF	0.25(5)	2.30(0.51)	0.73(14)

interactions characterized by high-momentum components, like AV18. In this sense, the absence of two-body currents in our NMEs may have a smaller impact than for *ab initio* methods relying on a single-particle basis expansion that deal with softer nuclear potentials.

The GCF-SM $0\nu\beta\beta$ matrix elements presented in this work rely on VMC calculations carried out with the AV18 + UX Hamiltonian, and the short-range GCF two-body function has consistently been computed with AV18. In future work we plan to study the NME dependence on the nuclear Hamiltonian of choice, including ones derived within chiral effective field theory. For instance, the local chiral Norfolk two- and three-body potentials can be readily incorporated in the GCF-SM method once the VMC calculations are carried out. On the other hand, including nonlocal potentials would require calculating transition densities for light nuclei with suitable many-body methods, like the no-core shell model [99,114].

A further development of the method is to improve the treatment of the tensor matrix element. This is especially important in view of a recent *ab initio* study that found relatively large tensor contributions compared with the SM [37]. This development will require disentangling the different p-wave contributions at short distances and additional analyses of the model independence of contact ratios. We also note that there are some differences between the SM and the VMC at intermediate and long distances that should be further studied to improve the accuracy of our predictions.

More generally, the GCF-SM approach, anchored on VMC calculations of light nuclei, can be applied to incorporating the effect of SRCs in a variety of nuclear quantities accessible by the nuclear SM. We envision computing the transition densities relevant for studying the role of correlations and two-body currents in single-β decay rates. As noted in Ref. [42], the two-body densities exhibit a universal, i.e., nucleus independent, behavior at short distance. Describing the contribution of the leading one-body current is more complicated, since the separation to short-range and long-range contributions is less obvious. Also, we plan on utilizing the GCF-SM method to analyze momentum distributions and spectral functions of nuclei of interest in the context of electron-scattering experiments and for the accelerator-based neutrino oscillation program.

ACKNOWLEDGMENTS

We would like to thank J.M. Yao for sharing with us the IT-NCSM calculations. The present research is supported by the U.S. Department of Energy, Office of Science, Office of Nuclear Physics, under Contract No. DE-AC02-06CH11357, the NUCLEI SciDAC program (A.L., R.B.W.), by the Laboratory Directed Research and Development program of Los Alamos National Laboratory under Project No. 20210763PRD1 (R.W.), and by the "Ramón y Cajal" program with Grant No. RYC-2017-22781, and Grants No. CEX2019-000918-M and No. PID2020-118758GB-I00 funded by MCIN/AEI/10.13039/501100011033 and, by "ESF Investing in your future" (P.S. and J.M.). The work of A.L. is also supported by the DOE Early Career Research Program award. Quantum Monte Carlo calculations were performed on the parallel computers of the Laboratory Computing Resource Center, Argonne National Laboratory, the computers of the Argonne Leadership Computing Facility via the INCITE grant "*Ab initio* nuclear structure and nuclear reactions," and the 2020/2021 ALCC grant "Chiral Nuclear Interactions from Nuclei to Nucleonic Matter."

APPENDIX A: ADDITIONAL SHELL MODEL INTERACTIONS

Table IV provides the values of the NMEs using additional SM interactions: GXPF1B for the decay of ^{48}Ca and JUN45 and JJ4BB for the decay of ^{76}Ge. As noted in the main body of the paper, these results are compatible within errors with those reported in Table III.

APPENDIX B: ISOSPIN SYMMETRY

As discussed above, due to isospin symmetry the integral $\int_0^\infty 4\pi r^2 \rho_F(r)$ should approximately vanish for isospin-changing transitions. Table V presents the values of this

TABLE V. Values of the integrals $\int_0^\infty 4\pi r^2 \rho_F(r)$ and $\int_0^\infty 4\pi r^2 \rho_{GT}(r)$ for isospin-changing decays ($\Delta T = 2$) using different methods. For the SM we use the KB3G interaction for $A = 48$, GCN2850 for $A = 76$, and GCN5082 for $A = 130$ and $A = 136$.

Transition	Method	$\int_0^\infty 4\pi r^2 \rho_F(r)$	$\int_0^\infty 4\pi r^2 \rho_{GT}(r)$
$^{12}\text{Be} \to {}^{12}\text{C}$	VMC_5	-0.00026	0.20
	WSS	-0.000021	-0.036
	WSS + GCF	0.010 ± 0.004	-0.06 ± 0.02
$^{48}\text{Ca} \to {}^{48}\text{Ti}$	WSS	0.000065	0.14
	WSS + GCF	0.009 ± 0.003	0.09 ± 0.02
$^{76}\text{Ge} \to {}^{76}\text{Se}$	HO	-0.000013	0.56
	HO(S) + GCF	0.018 ± 0.006	0.4 ± 0.1
$^{130}\text{Te} \to {}^{130}\text{Xe}$	HO	0.0000085	0.35
	HO(S) + GCF	0.028 ± 0.009	0.23 ± 0.05
$^{136}\text{Xe} \to {}^{136}\text{Ba}$	HO	0.000019	0.27
	HO(S) + GCF	0.020 ± 0.007	0.17 ± 0.04

integral for the isospin-changing decays using the VMC, SM, and GCF-SM approaches. For the VMC and SM calculations, $\int_0^\infty 4\pi r^2 \rho_F(r) \approx 10^{-4}$–$10^{-6}$. For the GCF-SM calculations, we obtain smaller cancellations of the order of 10^{-2}. To understand the origin of this result, we can compare the $A = 12$ F transition we obtain using the GCF-SM method with the VMC results (top panel of Fig. 4). At short distances there is a good agreement between the two calculations, while for longer distances there are some small differences. We note that Fig. 4 shows the $C_F^{0\nu}(r)$ density which includes the transition potential $V_F^{0\nu}(r)$. Asymptotically, this potential has the form $\approx 1/r$, and, therefore, the long-distance tail is suppressed in $C_F^{0\nu}(r)$. When we consider $\rho_F(r)$, the long-distance tail becomes more significant. We can therefore conclude that differences between the VMC and the SM in the long-range tail are the main reason for the $\int_0^\infty 4\pi r^2 \rho_F(r)$ values we obtain in the GCF-SM approach. Such differences are much less significant for the calculation of $0\nu\beta\beta$ NMEs due to the $1/r$ suppression, and therefore the value of this integral should not be regarded as an important criteria for the reliability of $0\nu\beta\beta$ NMEs.

The values of the integral $\int_0^\infty 4\pi r^2 \rho_{GT}(r)$ are also presented in Table V. Again, for $A = 12$ the disagreement between the VMC and GCF-SM values is driven by the long-range part (see Fig. 4). References [67,115] discuss the relevance of this integral, and its possible connection to $0\nu\beta\beta$ decay. For ^{48}Ca, ^{76}Ge, ^{130}Te, and ^{136}Xe, the GCF-SM values with uncertainties are in good agreement with the correlations presented in Ref. [115].

[1] W. H. Furry, Phys. Rev. **56**, 1184 (1939).
[2] J. Schechter and J. W. F. Valle, Phys. Rev. D: Part. Fields **25**, 2951 (1982).
[3] S. Dell'Oro, S. Marcocci, M. Viel, and F. Vissani, Adv. High Energy Phys. **2016**, 2162659 (2016).
[4] L. Cardani, SciPost Phys. Proc. **1**, 024 (2019).
[5] M. Agostini *et al.* (GERDA Collaboration), Phys. Rev. Lett. **125**, 252502 (2020).
[6] A. Gando *et al.* (KamLAND-Zen Collaboration), Phys. Rev. Lett. **117**, 082503 (2016); **117**, 109903(E) (2016).
[7] S. A. Kharusi *et al.* (nEXO Collaboration), arXiv:1805.11142.
[8] C. Adams *et al.* (NEXT Collaboration), J. High Energy Phys. 08 (2021) 164.
[9] N. Abgrall *et al.* (LEGEND Collaboration), arXiv:2107.11462.
[10] W. R. Armstrong *et al.* (CUPID Collaboration), arXiv:1907.09376.
[11] M. T. Mustonen and J. Engel, Phys. Rev. C **87**, 064302 (2013).
[12] F. Šimkovic, V. Rodin, A. Faessler, and P. Vogel, Phys. Rev. C **87**, 045501 (2013).
[13] J. Hyvärinen and J. Suhonen, Phys. Rev. C **91**, 024613 (2015).
[14] D.-L. Fang, A. Faessler, and F. Simkovic, Phys. Rev. C **92**, 044301 (2015).
[15] J. Menéndez, A. Poves, E. Caurier, and F. Nowacki, Nucl. Phys. A **818**, 139 (2009).
[16] Y. Iwata, N. Shimizu, T. Otsuka, Y. Utsuno, J. Menéndez, M. Honma, and T. Abe, Phys. Rev. Lett. **116**, 112502 (2016); **117**, 179902(E) (2016).
[17] M. Horoi and A. Neacsu, Phys. Rev. C **93**, 024308 (2016).
[18] L. Coraggio, A. Gargano, N. Itaco, R. Mancino, and F. Nowacki, Phys. Rev. C **101**, 044315 (2020).
[19] T. R. Rodríguez and G. Martínez-Pinedo, Phys. Rev. Lett. **105**, 252503 (2010).
[20] N. L. Vaquero, T. R. Rodríguez, and J. L. Egido, Phys. Rev. Lett. **111**, 142501 (2013).
[21] J. M. Yao, L. S. Song, K. Hagino, P. Ring, and J. Meng, Phys. Rev. C **91**, 024316 (2015).
[22] J. M. Yao and J. Engel, Phys. Rev. C **94**, 014306 (2016).
[23] J. Barea, J. Kotila, and F. Iachello, Phys. Rev. C **91**, 034304 (2015).
[24] F. F. Deppisch, L. Graf, F. Iachello, and J. Kotila, Phys. Rev. D **102**, 095016 (2020).
[25] E. Caurier, G. Martínez-Pinedo, F. Nowack, A. Poves, and A. P. Zuker, Rev. Mod. Phys. **77**, 427 (2005).
[26] T. Otsuka, A. Gade, O. Sorlin, T. Suzuki, and Y. Utsuno, Rev. Mod. Phys. **92**, 015002 (2020).
[27] B. A. Brown and B. H. Wildenthal, Annu. Rev. Nucl. Part. Sci. **38**, 29 (1988).
[28] J. Engel and J. Menéndez, Rep. Prog. Phys. **80**, 046301 (2017).
[29] P. Gysbers *et al.*, Nat. Phys. **15**, 428 (2019).
[30] W. T. Chou, E. K. Warburton, and B. A. Brown, Phys. Rev. C **47**, 163 (1993).
[31] B. H. Wildenthal, M. S. Curtin, and B. A. Brown, Phys. Rev. C **28**, 1343 (1983).
[32] G. Martínez-Pinedo, A. Poves, E. Caurier, and A. P. Zuker, Phys. Rev. C **53**, R2602 (1996).
[33] P. Pirinen and J. Suhonen, Phys. Rev. C **91**, 054309 (2015).
[34] S. Novario, P. Gysbers, J. Engel, G. Hagen, G. R. Jansen, T. D. Morris, P. Navrátil, T. Papenbrock, and S. Quaglioni, Phys. Rev. Lett. **126**, 182502 (2021).
[35] J. M. Yao, B. Bally, J. Engel, R. Wirth, T. R. Rodríguez, and H. Hergert, Phys. Rev. Lett. **124**, 232501 (2020).
[36] R. Wirth, J. M. Yao, and H. Hergert, Phys. Rev. Lett. **127**, 242502 (2021).
[37] A. Belley, C. G. Payne, S. R. Stroberg, T. Miyagi, and J. D. Holt, Phys. Rev. Lett. **126**, 042502 (2021).

[38] J. Carlson, S. Gandolfi, F. Pederiva, S. C. Pieper, R. Schiavilla, K. E. Schmidt, and R. B. Wiringa, Rev. Mod. Phys. **87**, 1067 (2015).
[39] H. Hergert, Front. Phys. **8**, 379 (2020).
[40] V. Cirigliano, W. Dekens, J. de Vries, M. L. Graesser, E. Mereghetti, S. Pastore, and U. van Kolck, Phys. Rev. Lett. **120**, 202001 (2018).
[41] V. Cirigliano, W. Dekens, J. De Vries, M. L. Graesser, E. Mereghetti, S. Pastore, M. Piarulli, U. van Kolck, and R. B. Wiringa, Phys. Rev. C **100**, 055504 (2019).
[42] G. B. King, L. Andreoli, S. Pastore, M. Piarulli, R. Schiavilla, R. B. Wiringa, J. Carlson, and S. Gandolfi, Phys. Rev. C **102**, 025501 (2020).
[43] S. Pastore, J. Carlson, V. Cirigliano, W. Dekens, E. Mereghetti, and R. B. Wiringa, Phys. Rev. C **97**, 014606 (2018).
[44] R. Weiss, B. Bazak, and N. Barnea, Phys. Rev. Lett. **114**, 012501 (2015).
[45] R. Weiss, B. Bazak, and N. Barnea, Phys. Rev. C **92**, 054311 (2015).
[46] R. Weiss, R. Cruz-Torres, N. Barnea, E. Piasetzky, and O. Hen, Phys. Lett. B **780**, 211 (2018).
[47] R. Cruz-Torres, D. Lonardoni, R. Weiss, M. Piarulli, N. Barnea, D. W. Higinbotham, E. Piasetzky, A. Schmidt, L. B. Weinstein, R. B. Wiringa, and O. Hen, Nat. Phys. **17**, 306 (2021).
[48] G. A. Miller and J. E. Spencer, Ann. Phys. (NY) **100**, 562 (1976).
[49] F. Šimkovic, A. Faessler, H. Müther, V. Rodin, and M. Stauf, Phys. Rev. C **79**, 055501 (2009).
[50] O. Benhar, R. Biondi, and E. Speranza, Phys. Rev. C **90**, 065504 (2014).
[51] X. B. Wang, A. C. Hayes, J. Carlson, G. X. Dong, E. Mereghetti, S. Pastore, and R. B. Wiringa, Phys. Lett. B **798**, 134974 (2019).
[52] G. Pantis and J. D. Vergados, Phys. Rep. **242**, 285 (1994).
[53] A. Faessler, W. A. Kaminski, G. Pantis, and J. D. Vergados, Phys. Rev. C **43**, R21 (1991).
[54] R. A. Sen'kov, M. Horoi, and B. A. Brown, Phys. Rev. C **89**, 054304 (2014).
[55] R. A. Sen'kov and M. Horoi, Phys. Rev. C **93**, 044334 (2016).
[56] V. Cirigliano, W. Dekens, E. Mereghetti, and A. Walker-Loud, Phys. Rev. C **97**, 065501 (2018); **100**, 019903(E) (2019).
[57] Z. Ye, J. Arrington, R. J. Hill, and G. Lee, Phys. Lett. B **777**, 8 (2018).
[58] A. S. Meyer, M. Betancourt, R. Gran, and R. J. Hill, Phys. Rev. D **93**, 113015 (2016).
[59] F. Šimkovic, G. Pantis, J. D. Vergados, and A. Faessler, Phys. Rev. C **60**, 055502 (1999).
[60] M. Kortelainen and J. Suhonen, Phys. Rev. C **75**, 051303(E) (2007).
[61] Z. Davoudi and S. V. Kadam, Phys. Rev. Lett. **126**, 152003 (2021).
[62] Z. Davoudi and S. V. Kadam, Phys. Rev. D **105**, 094502 (2022).
[63] V. Cirigliano, W. Dekens, J. de Vries, M. Hoferichter, and E. Mereghetti, Phys. Rev. Lett. **126**, 172002 (2021).
[64] V. Cirigliano, W. Dekens, J. de Vries, M. Hoferichter, and E. Mereghetti, J. High Energy Phys. 05 (2021)289.
[65] R. B. Wiringa, V. G. J. Stoks, and R. Schiavilla, Phys. Rev. C **51**, 38 (1995).
[66] M. Piarulli, L. Girlanda, R. Schiavilla, A. Kievsky, A. Lovato, L. E. Marcucci, S. C. Pieper, M. Viviani, and R. B. Wiringa, Phys. Rev. C **94**, 054007 (2016).
[67] F. Šimkovic, A. Smetana, and P. Vogel, Phys. Rev. C **98**, 064325 (2018).
[68] S. C. Pieper, AIP Conf. Proc. **1011**, 143 (2008).
[69] S. C. Pieper, K. Varga, and R. B. Wiringa, Phys. Rev. C **66**, 044310 (2002).
[70] B. S. Pudliner, V. R. Pandharipande, J. Carlson, S. C. Pieper, and R. B. Wiringa, Phys. Rev. C **56**, 1720 (1997).
[71] S. R. Stroberg, S. K. Bogner, H. Hergert, and J. D. Holt, Annu. Rev. Nucl. Part. Sci. **69**, 307 (2019).
[72] E. K. Warburton, B. A. Brown, and D. J. Millener, Phys. Lett. B **293**, 7 (1992).
[73] E. K. Warburton and B. A. Brown, Phys. Rev. C **46**, 923 (1992).
[74] J. Menéndez, J. Phys. G **45**, 014003 (2018).
[75] A. Poves, J. Sanchez-Solano, E. Caurier, and F. Nowacki, Nucl. Phys. A **694**, 157 (2001).
[76] M. Honma, T. Otsuka, and T. Mizusaki, RIKEN Accel. Prog. Rep. **41**, 32 (2008).
[77] M. Honma, T. Otsuka, T. Mizusaki, and M. Hjorth-Jensen, Phys. Rev. C **80**, 064323 (2009).
[78] B. A. Brown and A. F. Lisetskiy (private communication).
[79] E. Caurier, F. Nowacki, A. Poves, and K. Sieja, Phys. Rev. C **82**, 064304 (2010).
[80] J. Menéndez, N. Hinohara, J. Engel, G. Martínez-Pinedo, and T. R. Rodríguez, Phys. Rev. C **93**, 014305 (2016).
[81] L. Jokiniemi, B. Romeo, P. Soriano, and J. Menéndez, arXiv:2207.05108.
[82] E. Caurier, F. Nowacki, and A. Poves, Eur. Phys. J. A **36**, 195 (2008).
[83] M. Horoi and B. A. Brown, Phys. Rev. Lett. **110**, 222502 (2013).
[84] B. A. Brown, D. L. Fang, and M. Horoi, Phys. Rev. C **92**, 041301(R) (2015).
[85] J. Suhonen, *From Nucleons to Nuclei, Concepts of Microscopic Nuclear Theory*, Theoretical and Mathematical Physics, 1st ed. (Springer, Berlin, Heidelberg 2007).
[86] N. Schwierz, I. Wiedenhover, and A. Volya, arXiv:0709.3525.
[87] R. Cruz-Torres, A. Schmidt, G. Miller, L. Weinstein, N. Barnea, R. Weiss, E. Piasetzky, and O. Hen, Phys. Lett. B **785**, 304 (2018).
[88] R. Roth, H. Hergert, P. Papakonstantinou, T. Neff, and H. Feldmeier, Phys. Rev. C **72**, 034002 (2005).
[89] R. Weiss, I. Korover, E. Piasetzky, O. Hen, and N. Barnea, Phys. Lett. B **791**, 242 (2019).
[90] A. Schmidt *et al.* (CLAS Collaboration), Nature (London) **578**, 540 (2020).
[91] J. Pybus, I. Korover, R. Weiss, A. Schmidt, N. Barnea, D. Higinbotham, E. Piasetzky, M. Strikman, L. Weinstein, and O. Hen, Phys. Lett. B **805**, 135429 (2020).
[92] M. Duer *et al.* (CLAS Collaboration), Phys. Rev. Lett. **122**, 172502 (2019).
[93] R. Weiss, A. W. Denniston, J. R. Pybus, O. Hen, E. Piasetzky, A. Schmidt, L. B. Weinstein, and N. Barnea, Phys. Rev. C **103**, L031301 (2021).
[94] R. Weiss, B. Bazak, and N. Barnea, Eur. Phys. J. A **52**, 92 (2016).
[95] R. Weiss, E. Pazy, and N. Barnea, Few-Body Syst. **58**, 9 (2017).

[96] R. Weiss, A. Schmidt, G. A. Miller, and N. Barnea, Phys. Lett. B **790**, 484 (2019).
[97] O. Hen, D. W. Higinbotham, G. A. Miller, E. Piasetzky, and L. B. Weinstein, Int. J. Mod. Phys. E **22**, 1330017 (2013).
[98] A. J. Tropiano, S. K. Bogner, and R. J. Furnstahl, Phys. Rev. C **104**, 034311 (2021).
[99] J. M. Yao, A. Belley, R. Wirth, T. Miyagi, C. G. Payne, S. R. Stroberg, H. Hergert, and J. D. Holt, Phys. Rev. C **103**, 014315 (2021).
[100] N. Hinohara and J. Engel, Phys. Rev. C **90**, 031301(R) (2014).
[101] J. Menéndez, T. R. Rodríguez, G. Martínez-Pinedo, and A. Poves, Phys. Rev. C **90**, 024311 (2014).
[102] J. M. Yao, J. Meng, Y. F. Niu, and P. Ring, Prog. Part. Nucl. Phys. **126**, 103965 (2022).
[103] E. Caurier, J. Menéndez, F. Nowacki, and A. Poves, Phys. Rev. Lett. **100**, 052503 (2008).
[104] M. Horoi, A. Neacsu, and S. Stoica, Phys. Rev. C **106**, 054302 (2022).
[105] E. Caurier, A. Poves, and A. Zuker, Phys. Lett. B **252**, 13 (1990).
[106] E. Caurier, A. P. Zuker, A. Poves, and G. Martínez-Pinedo, Phys. Rev. C **50**, 225 (1994).
[107] L. Jokiniemi, P. Soriano, and J. Menéndez, Phys. Lett. B **823**, 136720 (2021).
[108] J. Engel, J. Carlson, and R. B. Wiringa, Phys. Rev. C **83**, 034317 (2011).
[109] T. R. Richardson, M. R. Schindler, S. Pastore, and R. P. Springer, Phys. Rev. C **103**, 055501 (2021).
[110] S. Pastore, A. Baroni, J. Carlson, S. Gandolfi, S. C. Pieper, R. Schiavilla, and R. B. Wiringa, Phys. Rev. C **97**, 022501(R) (2018).
[111] J. Menéndez, D. Gazit, and A. Schwenk, Phys. Rev. Lett. **107**, 062501 (2011).
[112] J. Engel, F. Simkovic, and P. Vogel, Phys. Rev. C **89**, 064308 (2014).
[113] L.-J. Wang, J. Engel, and J. M. Yao, Phys. Rev. C **98**, 031301(R) (2018).
[114] R. A. M. Basili, J. M. Yao, J. Engel, H. Hergert, M. Lockner, P. Maris, and J. P. Vary, Phys. Rev. C **102**, 014302 (2020).
[115] N. Shimizu, J. Menéndez, and K. Yako, Phys. Rev. Lett. **120**, 142502 (2018).